Climb of jogs as a rate-limiting process of screw dislocation motion in olivine dislocation creep

Lin Wang[a, b] and Tomoo Katsura[a, c]

[a] Bayerisches Geoinstitut, University of Bayreuth, 95440 Bayreuth, Germany.

[b] Geophysical laboratory, Carnegie institution for Science, Washington D.C., 20015, U.S.A.

[c] Center for High Pressure Science and Technology Advanced Research, Beijing, 100094, China

* Corresponding author.

E-mail address: liwang@carnegiescience.edu

Abstract

Dislocation recovery experiments were conducted on predeformed olivine single crystals at temperatures of 1,450 to 1,760 K, room pressure, and oxygen partial pressures near the Ni-NiO buffer to determine the annihilation rate constants for [001](010) edge dislocations. The obtained rate constants were found to be comparable to those of previously determined [001] screw dislocations. The activation energies for the motion of both dislocations are identical. This result suggests that the motion of screw dislocations in olivine is not controlled by cross-slip but by the same rate-limiting process of the motion of edge dislocations, i.e., climb, under low-stress, high-temperature conditions. The diffusivity derived from dislocation climb indicates that dislocation recovery is controlled by Si pipe diffusion, rather than Si lattice diffusion. Our results suggest that the conventional climb-controlled model for olivine can be applied to motions of not only edge but also screw dislocations. Therefore, the previous proposed cross-slip model cannot explain the softness of asthenosphere. ~~The diffusivity derived from dislocation climb indicates that dislocation recovery is controlled by pipe diffusion. The conventional climb-controlled model for olivine can be applied to the motions of not only edge but also screw dislocations. The softness of the asthenosphere cannot be explained by cross-slip controlled olivine dislocation creep.~~

Keywords: dislocation recovery, dislocation creep, temperature dependence, climb controlled model, asthenosphere

Introduction

Geophysical observations regarding geoid (e.g., Hager, 1991) and postglacial rebound (e.g., Peltier, 1998) have suggested that a soft asthenosphere underlies a rigid lithosphere. Geodynamic modeling (e.g., Becker, 2017; Craig and McKenzie, 1986) have also suggested the same conclusion.

The reason for the presence of soft asthenosphere is under debate. Although the simplest explanation cites a weakening of materials due to high temperatures, the results of deformation experiments conducted on dry peridotite implied that high temperatures are insufficient to explain the softness of the asthenosphere (Hirth and Kohlstedt, 2003). ~~Although a~~A popular explanation refers to the hydrous weakening of olivine (e.g., Mackwell et al., 1985; Hirth and Kohlstedt, 2003). However, ~~-~~ this has been refuted by recent Si self-diffusion experiments (Fei et al., 2016; Fei et al., 2013) based on the assumption that dislocation creep is controlled by diffusion. Another possible explanation was proposed by Poirier and Vergobbi (1978). The authors suggested that if the cross-slip of dissociated screw dislocations controls olivine dislocation creep, the estimated upper-mantle viscosity would be one order of magnitude lower than that predicted by the climb-controlled model in a stress range from 10 to 100 bar. This property may explain the softness of the asthenosphere. However, no experimental study has tested this hypothesis.

Neither diffusion nor deformation experiments can identify the rate-limiting process of motions of screw dislocations. Diffusion does not involve motions of dislocations. Although it is theoretically possible to determine the rate-limiting process of dislocation motions by examining the stress dependence of creep rates (e.g., Hirth and Kohlstedt, 2003), the stress ranges applied in deformation experiments are too narrow. The conventionally used stress exponent of 3.5 for dislocation creep implies a pipe diffusion-controlled mechanism (Hirth and Kohlstedt, 2003, 2015). However, such experiments have a stress range only from 100 to 224 MPa. On the other hand, Kohlstedt and Goetze (1974) found that the stress exponent increases with increasing stress. Poirier (1985, P.139) found that the stress exponent of olivine single crystal dislocation creep varies from 2.6 to 3.7 in different studies.

In the present study, we conducted dislocation recovery experiments on [001](010) edge dislocations and compared the results with those of [001](010) screw dislocations given by Wang et al. (2016). During recovery, dislocations move on (glide) and out of the slip plane (climb, cross-slip) successively under the influence of internal stress. Therefore, the activation energy determined by this method represents that of the rate-limiting process of dislocation motions. Although the model developed by Poirier and Vergobbi (1978) ~~i~~was based on [100] screw dislocations, the important point in their model is the dissociation, rather than Burgers vector of dislocations. Because dissociation of [001] screw dislocations have been confirmed in olivine (Vander Sande and Kohlstedt, 1976), [001] screw dislocation can be used to test this hypothesis. In addition, most of [100] dislocations~~these~~ have an edge character at temperatures of less than 1350 °C (Bai and Kohlstedt, 1992; Wang et al., 2016). ~~On the other hand~~while~~,~~ [001] dislocations has similar density of edge and screw components (Wang et al., 2016).~~the similar density of edge and screw dislocations in the [001](010) slip system (Wang et al., 2016)~~ This indicates the equivalent importance of both types of dislocations in this slip system. Therefore, we focus on ~~this~~ the [001](010) slip system in this study (hereafter called ***c***-dislocations).

Experimental Procedure

The same Pakistan olivine and sample preparation procedures as those of Wang et al. (2016) were employed in this study. The composition of olivine was reported by Gose et al. (2010). The experimental setup used is similar to that used in Wang et al. (2016). The olivine single crystal was oriented by X-ray diffraction and electron backscattered diffraction (EBSD) and then placed in the

cell assembly such that the [001] direction and (010) plan were parallel to the shear direction and plane, respectively.

Dislocations with the [001] Burgers vector on the (010) plane were produced by experimental deformation using a Kawai-type multianvil apparatus at the University of Bayreuth. The sample assembly was first pressurized to 3 GPa with a press load of 3.6 MN and then heated to a temperature of 1,600 K and held for 15 min to sinter crushable alumina. After this, the assembly was further compressed to a press load of 3.9 MN for 15 min to deform the sample. After deformation, the sample was quenched by switching off the heating power and then decompressed to room pressure for more than 16 hours. Transmission electronic microscopy (TEM) results presented by Wang et al. (2016) found the [001](010) slip system to be successfully activated and dominant using this procedure. The ratio of screw to edge dislocations was 3:2 as reported by Wang et al. (2016).

The deformed olivine crystals were cut into eight cubic pieces and paired into four groups, in which the two pieces in each group shared a common (100) plane. One piece from each pair was used to determine the initial dislocation density while the other was used to determine dislocation density after annealing. The annealing experiments were conducted at ambient pressure and temperatures of 1,460 to 1,760 K for 35 min to 24 hours using a gas mixing furnace. The oxygen partial pressure was controlled at 10^{-6}-10^{-8} MPa, which is near the Ni-NiO buffer, using a CO-CO_2 gas mixture. Table 1 summarizes the conditions of the annealing experiments.

Dislocations were observed using the oxidation decoration technique (Kohlstedt et al., 1976, Karato 1987). Corresponding areas away from subgrain boundaries on the common (100) plane in initial and annealed pieces of the same group were observed to determine the change in dislocation

density before and after annealing. Although dislocations exist mainly as loops in crystals, the high lattice friction in the [001](010) slip system makes the screw and edge components nearly straight in this slip system (Bai and Kohlstedt 1992, sample deformed in $[011]_c$ orientation, Wang et al., 2016, ***c***-deformed sample). This enable us to distinguish the characters of dislocations by using line geometry of dislocations (Ogawa and Karato, 1989). Since [001](010) edge dislocations elongate in the [100] direction, these dislocations show dots contrasted on the (100) plane in backscattered images after decoration. The number of dots per unit area was counted as the dislocation density.

Annihilation rate constants were calculated via second-order dislocation recovery kinetics (Karato and Ogawa, 1982; Kohlstedt et al., 1980; Wang et al., 2016)

$$k = \frac{\frac{1}{\rho_f} - \frac{1}{\rho_i}}{t}, \qquad (2)$$

where ρ_f and ρ_i are the dislocation densities after and before annealing, respectively, and t is the annealing time. Due to the thermally activated process, the dislocation annihilation rate constant is assumed to follow the Arrhenius relationship:

$$k = k_0 \exp\left(\frac{-E}{RT}\right) \qquad (3)$$

where k_0 is a constant, E is the activation energy of dislocation annihilation, T is temperature, and R is the gas constant.

Results

Table 1 shows experimental results together with the annealing conditions. Dislocation density in the samples before deformation is less than 0.0004 μm^{-2}, which is negligible in comparison to the dislocation density after deformation (Table 1). Figure 1 a and b shows back-scattered electron

images of decorated dislocations in corresponding areas in the samples from the same pair before and after annealing, respectively. ***c***-screw dislocations appear as lines and ***c***-edge dislocations appear as dots on the (100) plane due to their geometries. A decrease in dislocation density was observed by comparing the images before and after annealing. The water content in the samples before and after annealing was below the detection limit of infrared spectroscopy. The transmission electron microscope images of the dislocation structures after deformation are given in Fig. 4 in Wang et al. (2016).

Figure 1c plots the logarithmic rate constants of ***c***-edge dislocation annihilation against the reciprocal temperature. The results from the previous dislocation recovery experiments on *c*-screw dislocations (Wang et al., 2016) and of other studies on dislocation recovery kinetics are also plotted in this figure. The dislocation annihilation rate constants of ***c***-edge and ***c***-screw dislocations are comparable, but those of the ***c***-screw are about half an order of magnitude higher than those of the ***c***-edge. The temperature dependences for these two dislocations are identical. Their activation energies are $E_{\text{c-edge}}$ = 400 ± 20 kJ/mol and $E_{\text{c-screw}}$ = 400 ± 30 kJ/mol for the ***c***-edge and ***c***-screw, respectively.

Discussion

The identical activation energies of annihilation rate constants of the ***c***-edge and ***c***-screw dislocations indicate that the motions of both dislocations are controlled by the same mechanism. Although many transport properties of olivine exhibit activation energies of 300 to 500 kJ/mol (e.g., Dohmen et al., 2002, 529 ± 41 kJ/mol for silicon self-diffusion, 338 ± 14 kJ/mol for oxygen self-diffusion), they are distinct from those determined in this study (see also the slope in Fig. 3 and

143 references therein). The high accuracy of activation energies obtained in previous studies and the
144 present one allows us to distinguish the rate-limiting mechanisms of different processes.

145 The motion of edge dislocations is controlled by climb at high temperatures and low stresses
146 (e.g., Hull and Bacon, 2001; Kohlstedt, 2006). However, the motion of a pure screw dislocation
147 does not involve climb because screw segments have no specific slip plane (Hull and Bacon, 2001).
148 Since jogs in screw dislocations have an edge character, we propose that the motion of screw
149 dislocation is controlled by the climb of jogs (Fig. 2). A screw dislocation can form a jog by cross-
150 slips to overcome obstacles that it meets during glide (Fig. 2A and 2B). The slip plane of the jog is
151 defined by its dislocation line (***J***) and the Burgers vector (***b***), which is indicated by the yellow plane.
152 The parent screw dislocation glides in the *y* direction, and therefore the jog needs to climb in the *y*
153 direction to move along with its parental dislocation so that the screw dislocation can go through the
154 obstacle (Fig. 2C). This climb of jogs should serve as the rate-limiting process of screw dislocation
155 motions.

156 It should be noted that although the climb of edge dislocation and jog motion of screw
157 dislocation are essentially the same, the density of climbing parts on edge dislocations and that of
158 jogs on screw dislocations may be different, creating differences in the magnitudes of rate
159 constants. Thus, only the slope in the Arrhenius plot can serve as a fingerprint of the essential
160 mechanism of rate-limiting processes in dislocation recovery experiments.

161 Since climb is controlled by diffusion, the diffusivities derived from annihilation rate constant
162 D^R (based on Karato and Ogawan, 1989) were compared with those of silicon and oxygen diffusion
163 in olivine (Fig. 3). None of these data fit D^R well. Instead, D^R falls between silicon lattice and grain
164 boundary diffusivities. This result indicates that the dislocation climb in olivine may be controlled

by pipe diffusion. Vacancies, dislocations and grain boundaries are 0-, 1-, and 2-dimensional defects, respectively, the structure distortion near these defects should increase consequently and accordingly the associated Si diffusivity should increase. In addition, the activation energy of D^R obtained in this study is between those of Si lattice (540 kJ/mol, Dohmen et al., 2002) and grain boundary diffusion (~200 kJ/mol, Fei et al., 2015). This result is also consistent with the hypothesis that pipe diffusion controls dislocation climb (Hirth and Kohlstedt, 2015). Although there are no data for pipe diffusion in olivine, the fact that the diffusion coefficient and activation energy of pipe diffusion fall between those of lattice and grain boundary diffusion is well established for oxides (Frost and Ashby, 1983, Table 12.1). The low activation energy of oxygen lattice diffusion (~340 kJ/mol, Dohmen et al., 2002) rules out the possibility that oxygen diffusion controls dislocation climb.

Implications

Our results suggested that the conventional climb model can be used to dislocation motions in olivine regardless of dislocation characters. Although only [001] dislocation is studied in this study, the conclusion can be applied to dislocations with different Burgers vectors in olivine. The cross-slip model requires the recombination of dissociated screw dislocations. If the dissociation distance between two partial dislocations is large, the recombination is difficult. In this case, the cross-slip of screw dislocations can be a rate-limiting process (Poirier, 1976). Previous study (Vander Sande and Kohlstedt, 1976) has revealed that the dissociation distances of [001] and [100] dislocation are similar (~4 nm). Therefore, cross-slip cannot be the rate-limiting process for both [100] and [001] dislocations judging from present study. Although dissociation of [010] dislocations has been

reported (Fujino et al., 1993), its low abundance makes its effect on olivine dislocation creep less important.

~~It has been proposed that~~The observation that screw dislocation motion in olivine is controlled by climb of jogs indicates that the softness of the asthenosphere ~~can~~ cannot be attributed to the cross-slip controlled dislocation creep of olivine (Poirier and Vergobbi, 1978). Other factors, such as melt and water, could explain the softness of asthenosphere (Hirth and Kohlstedt, 2003). Although this explanation is refuted by Si lattice diffusion (Fei et al., 2013), our results indicate that dislocation climb in olivine is controlled by pipe rather than lattice diffusion under dry conditions. Further study on the water effect on dislocation recovery could reconcile the discrepancy between deformation and diffusion experiments results.

~~However, this hypothesis has never been tested. The present study demonstrates that the motion of [001] screw dislocations is controlled by the climb of jogs rather than cross-slip, suggesting that the cross-slip model is not applicable for such dislocations in olivine. Although the cross-slip model is based on [100] dislocations, study of the [001](010) slip system is more relevant to asthenosphere conditions. Dislocation structure analyses indicate that most [100](010) dislocations have an edge character (Bai and Kohlstedt, 1992, Wang et al., 2016), indicating that olivine dislocation creep cannot be controlled by motions of [100] screw dislocation. On the other hand, the similar density (Wang et al., 2016) of edge and screw dislocations in the [001](010) slip system indicates that both kinds of dislocations are important. Moreover, deformation experiments (e.g., Raterron et al., 2007) suggest that this slip system dominates at high pressuresTherefore, we conclude that the cross-slip of screw dislocations cannot control the dislocation creep of olivine and~~

~~accordingly cannot explain the softness of asthenosphere. The climb-controlled model can be used in olivine dislocation creep regardless of dislocation characters.~~

~~The viscosity of the asthenosphere is extrapolated from dry olivine creep data using a climb model is orders of magnitude higher than the estimated value drawn through geophysical observation (Hirth and Kohlstedt 2003). The hydrous weakening of olivine has been proposed to explain this discrepancy (e.g., Mackwell et al., 1985; Hirth and Kohlstedt, 2003), but this has been refuted by recent Si diffusion experiments (Fei et al., 2016; Fei et al., 2013). However, this study indicates that pipe diffusion rather than lattice or grain boundary diffusion may control the dislocation motions. This conclusion may explain the discrepant results of deformation and diffusion experiments. Further studies on the effect of water on dislocation recovery or pipe diffusion in olivine are needed to identify the effect of water on olivine rheology and to better explain the softness of the asthenosphere~~.

Acknowledgments

We thank H. Fischer and R. Njul of BGI for the sample and for assembly preparation. This research was supported through DFG grants to TK (KA3434-3/1, KA3434-3/2, KA3434-7/1 and KA3434-8/1) and with the annual budget of BGI. All data used in this paper are given in Table 1 and plotted in Fig. 1c and have been archived at Earth and Space Science Open Archive doi.org/10.1002/essoar.10501470.1.

References

Bai, Q., and Kohlstedt, D. L., 1992, High-temperature creep of olivine single crystals, 2. dislocation structures: Tectonophysics, v. 206, no. 1–2, p. 1-29.

Becker, T. W., 2017, Superweak asthenosphere in light of upper mantle seismic anisotropy: Geochemistry, Geophysics, Geosystems.

Craig, C. H., and McKenzie, D., 1986, The existence of a thin low-viscosity layer beneath the lithosphere: Earth and Planetary Science Letters, v. 78, no. 4, p. 420-426.

Dohmen, R., Chakraborty, S., and Becker, H.-W. (2002) Si and O diffusion in olivine and implications for characterizing plastic flow in the mantle. Geophysical Research Letters, 29(21), 2030.

Farver, J.R., and Yund, R.A. (2000) Silicon diffusion in forsterite aggregates: Implications for diffusion accommodated creep. Geophysical Research Letters, 27(15), 2337-2340.

Fei, H., Koizumi, S., Sakamoto, N., Hashiguchi, M., Yurimoto, H., Marquardt, K., Miyajima, N., Yamazaki, D., and Katsura, T., 2016, New constraints on upper mantle creep mechanism inferred from silicon grain-boundary diffusion rates: Earth and Planetary Science Letters, v. 433, p. 350-359.

Fei, H., Wiedenbeck, M., Yamazaki, D., and Katsura, T., 2013, Small effect of water on upper-mantle rheology based on silicon self-diffusion coefficients: Nature, v. 498, no. 7453, p. 213.

Frost, H.J. and M.F. Ashby, Deformation mechanism maps: the plasticity and creep of metals and ceramics. 1982: Pergamon press.

Fujino, K., H. Nakazaki, H. Momoi, S.-i. Karato, and D. L. Kohlstedt (1993), TEM observation of dissociated dislocations with b=[010] in naturally deformed olivine, *Physics of the earth and planetary interiors*, *78*(1-2), 131-137.

Gose, J., Schmaedicke, E., Markowitz, M., and Beran, A., 2010, OH point defects in olivine from Pakistan: Mineralogy and Petrology, v. 99, no. 1-2, p. 105-111.

Hager, B. H., 1991, Mantle viscosity: A comparison of models from postglacial rebound and from the geoid, plate driving forces, and advected heat flux, Glacial isostasy, sea-level and mantle rheology, Springer, p. 493-513.

Hirth, G., and Kohlstedt, D., 2003, Rheology of the Upper Mantle and the Mantle Wedge: A View from the Experimentalists, Inside the Subduction Factory, American Geophysical Union, p. 83-105.

Hirth, G., and Kohlstedt, D., 2015, The stress dependence of olivine creep rate: Implications for extrapolation of lab data and interpretation of recrystallized grain size: Earth and Planetary Science Letters, v. 418, p. 20-26.

Hull, D., and Bacon, D. J., 2001, Introduction to dislocations, Butterworth-Heinemann. P.257

Karato, S., and Ogawa, M., 1982, High-pressure recovery of olivine: implications for creep mechanisms and creep activation volume: Physics of the Earth and Planetary Interiors, v. 28, no. 2, p. 102-117.

Karato, S., Scanning electron microscope observation of dislocations in olivine. Physics and Chemistry of Minerals, 1987. 14(3): p. 245-248.

Kohlstedt, D.L., et al., New Technique for Decorating Dislocations in Olivine. Science, 1976. 191(4231): p. 1045-1046.

Kohlstedt, D., Nichols, H., and Hornack, P., 1980, The effect of pressure on the rate of dislocation recovery in olivine: Journal of Geophysical Research: Solid Earth (1978–2012), v. 85, no. B6, p. 3122-3130.

Kohlstedt, D. L., 2006, The Role of Water in High-Temperature Rock Deformation: Reviews in Mineralogy and Geochemistry, v. 62, no. 1, p. 377-396.

Kohlstedt, D. L., and Goetze, C., 1974, Low-stress high-temperature creep in olivine single crystals: Journal of Geophysical Research, v. 79, no. 14, p. 2045-2051.

Mackwell, S.J., Kohlstedt, D.L., and Paterson, M.S. (1985) The role of water in the deformation of olivine single-crystals. Journal of Geophysical Research-Solid Earth and Planets, 90(NB13), 1319-1333.Peltier, W., 1998, Postglacial variations in the level of the sea: Implications for climate dynamics and solid−earth geophysics: Reviews of Geophysics, v. 36, no. 4, p. 603-689.

Poirier, J. (1976), On the symmetrical role of cross-slip of screw dislocations and climb of edge dislocations as recovery processes controlling high-temperature creep, *Revue de Physique Appliquée*, *11*(6), 731-738.

Poirier, J.-P., 1985, Creep of crystals: high-temperature deformation processes in metals, ceramics and minerals, Cambridge University Press.

Poirier, J.-P., and Vergobbi, B., 1978, Splitting of dislocations in olivine, cross-slip-controlled creep and mantle rheology: Physics of the Earth and Planetary Interiors, v. 16, no. 4, p. 370-378.

Raterron, P., Chen, J., Li, L., Weidner, D., and Cordier, P. (2007) Pressure-induced slip-system transition in forsterite: Single-crystal rheological properties at mantle pressure and temperature. American Mineralogist, 92(8-9), 1436-1445.

Vander Sande, J., and D. Kohlstedt (1976), Observation of dissociated dislocations in deformed olivine, *Philosophical Magazine*, *34*(4), 653-658.

Wang, L., Blaha, S., Pintér, Z., Farla, R., Kawazoe, T., Miyajima, N., Michibayashi, K., and Katsura, T., 2016, Temperature dependence of [100](010) and [001](010) dislocation mobility in natural olivine: Earth and Planetary Science Letters, v. 441, p. 81-90.

Weertman, J., 1955, Theory of Steady−State Creep Based on Dislocation Climb: Journal of Applied Physics, v. 26, no. 10, p. 1213-1217.

Figure and table captions

Figure 1. BEIs showing the dislocation density (a) before and (b) after annealing at 1760 K for 35 min. The images were taken on the (100) plane. Screw and edge dislocations are shown as lines and dots, respectively, due to the geometries of their dislocation lines. The yellow scale bar denotes 2 μm. (c) Logarithmic dislocation annihilation rate constants of ***c***-edge dislocations versus reciprocal temperature. The annihilation rate constants of ***c***-screw dislocations from Wang et al. (2016) are plotted together. The activation energies for both dislocations are identical, i.e., 400 kJ/mol. Previous results on dislocation recovery are also plotted for comparison.

Figure 2. A schematic diagram showing the jog-climb controlled motion of a screw dislocation. (a) The screw dislocation (blue line) is elongated in the *x* direction, which is parallel to its Burgers vector ***b***, and glides in the *y* direction. The blue dot represents the obstacle that the screw dislocation meets during glide. (b) A jog (red segment) elongated in the *z* direction is produced on the screw dislocation to overcome the obstacle. This jog has an edge nature with the same Burgers vector ***b*** as that of the parental screw dislocation. The yellow area indicates the glide plane of the jog, which is normal to the *y* direction. (c) The jog has to climb out of its glide plane to move along with its parental screw dislocation.

Figure 3. Logarithmic diffusivity derived from dislocation annihilation rate constants of ***c***-edge and ***c***-screw dislocations versus reciprocal temperature. Si and O lattice and grain boundary diffusivities are plotted together.

Table 1. Summary of the experimental conditions and results.

330 Table 1. Summary of the experimental conditions and results*.

331

[001](010) edge dislocation						
Sample	T (K)	Annealing time (h)	$\log(f_{O_2}, 10^5\,\mathrm{Pa})$	ρ_i (μm^{-2})	ρ_f (μm^{-2})	$\log(k, m^2 s^{-1})$
Z1643-1	1763	0.58	-4.9	1.60±0.13	0.29±0.01	-14.87±0.03
				0.97±0.13	0.22±0.01	-14.77±0.03
Z1643-2	1673	2.5	-5.7	1.49±0.04	0.36±0.06	-15.63±0.09
				1.13±0.12	0.31±0.03	-15.58±0.05
Z1643-3	1473	24	-7.7	1.33±0.15	0.73±0.05	-17.14±0.09
				0.35±0.03	0.29±0.01	-17.22±0.27

332 * different ρ_i and ρ_f values of each sample correspond to different areas

333

334 Figure 1.

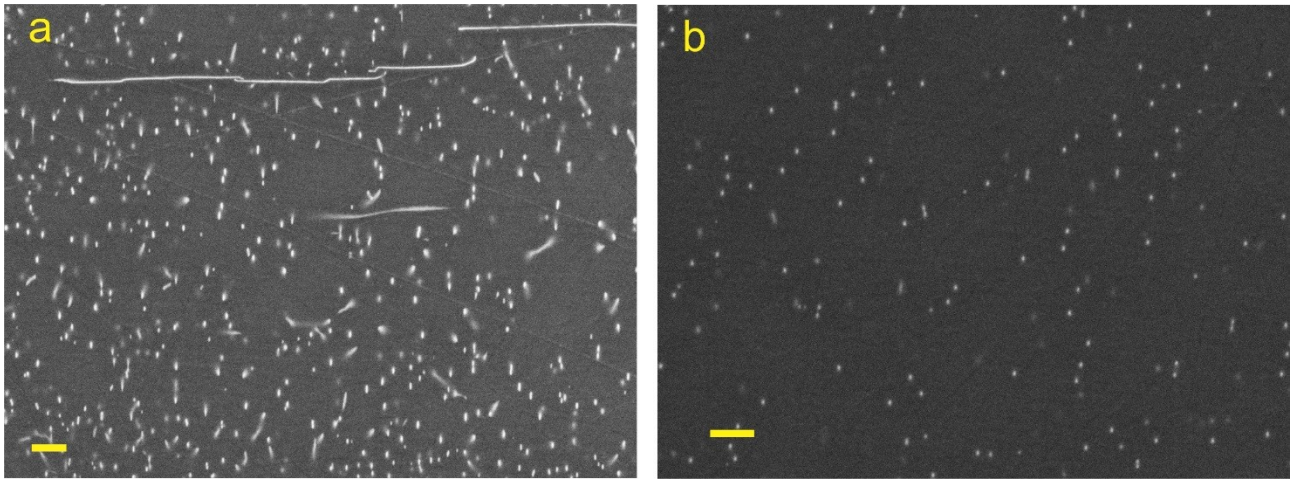

335

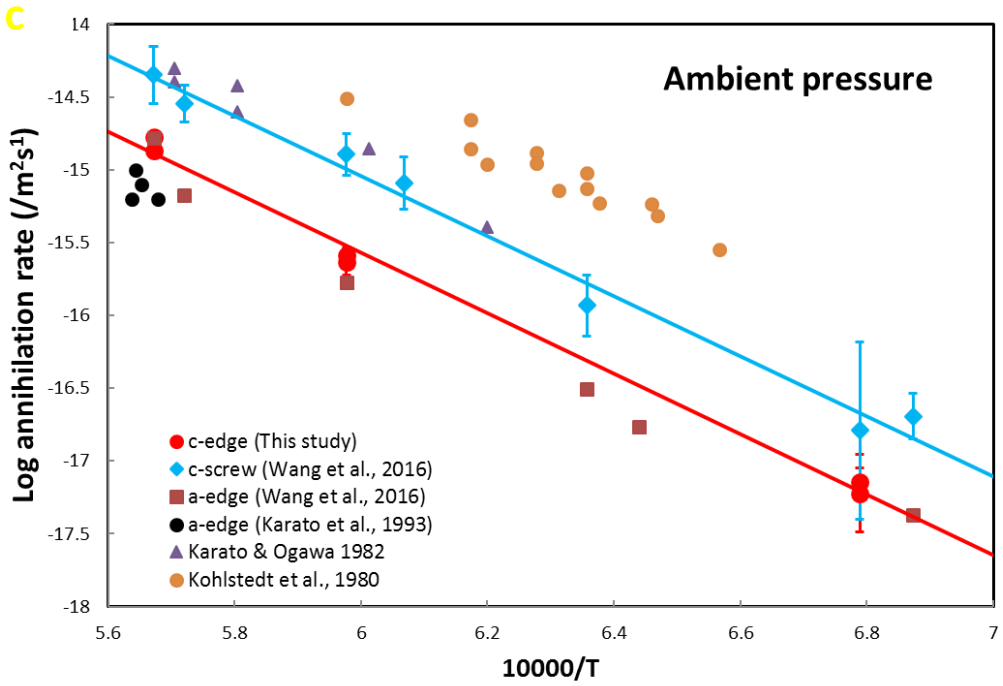

336

337

338

339 Figure 2.

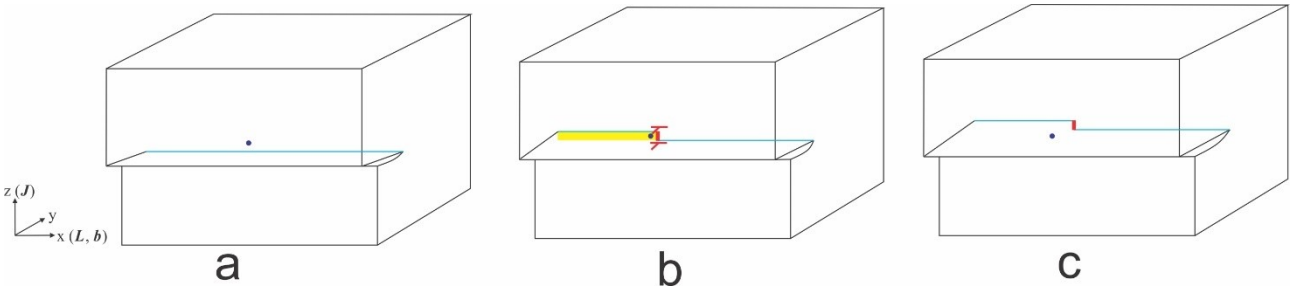

340

341

342 Figure 3.

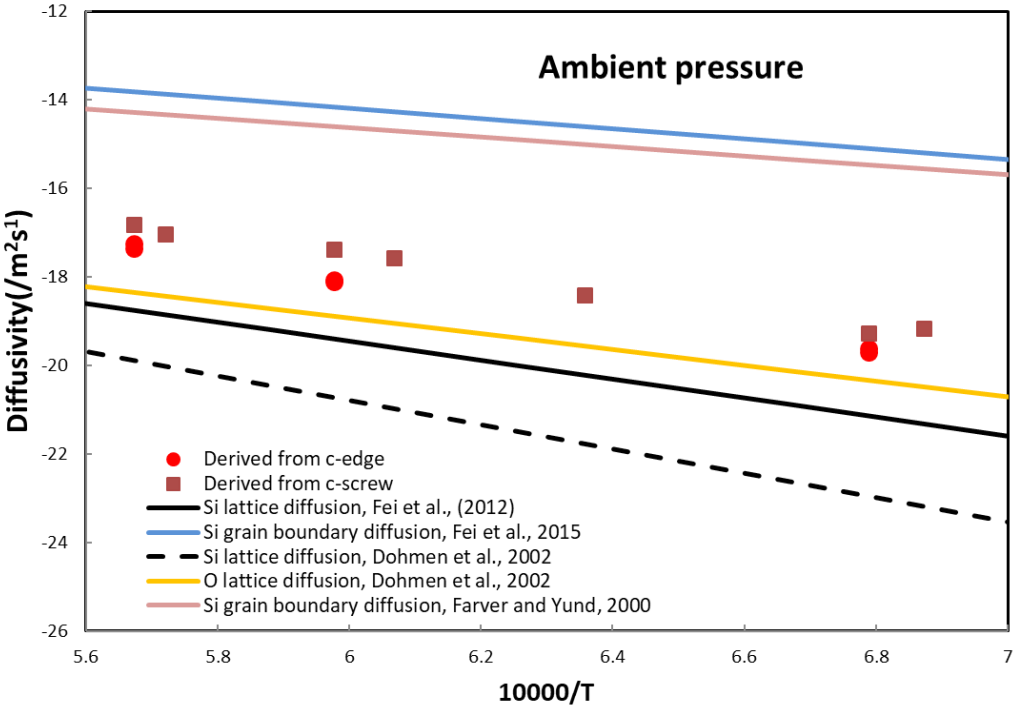

343